NANO LETTERS

Letter

pubs.acs.org/NanoLett

Atomic Calligraphy: The Direct Writing of Nanoscale Structures Using a Microelectromechanical System

Matthias Imboden,[†] Han Han,[‡] Jackson Chang,[†] Flavio Pardo,[§] Cristian A. Bolle,[§] Evan Lowell,[∥] and David J. Bishop*,[†,‡,⊥]

[†]Electrical and Computer Engineering and [‡]Department of Physics, Boston University, Boston, Massachusetts 02215, United States

[§]SLIM Line, Bell Laboratories, Alcatel-Lucent, Murray Hill, New Jersey 07974, United States

[∥]Department of Mechanical Engineering, Boston University, Boston, Massachusetts 02215, United States

[⊥]Division of Materials Science and Engineering, Boston University, Brookline, Massachusetts 02446, United States

Supporting Information

ABSTRACT: We present a microelectromechanical system (MEMS) based method for the resist-free patterning of nanostructures. Using a focused ion beam to customize larger MEMS machines, we fabricate apertures with features less than 50 nm in diameter on plates that can be moved with nanometer precision over an area greater than 20 × 20 μm^2. Depositing thermally evaporated gold atoms though the apertures while moving the plate results in the deposition of nanoscale metal patterns. Adding a shutter positioned micrometers above the aperture enables high speed control of not only where but also when atoms are deposited. With this shutter, different-sized apertures can be opened and closed selectively for nanostructure fabrication with features ranging from nano- to micrometers in scale. The ability to evaporate materials with high precision, and thereby fabricate circuits and structures in situ, enables new kinds of experiments based on the interactions of a small number of atoms and eventually even single atoms.

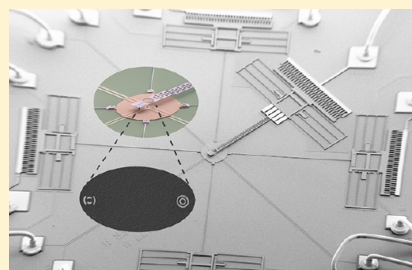

KEYWORDS: *MEMS, NEMS, nanotechnology, fab on a chip, nanofabrication*

In conventional lithography methods, a large amount of material is deposited or grown, and subsequently much of the material is removed, leaving the desired pattern. This method no longer works when the number of atoms wanted in a device is reduced to the level of single or few atoms. This is certainly true for optical and e-beam lithography.[1,2] The microelectromechanical system (MEMS) devices we present here allow for full patterning control of the amount and location of a desired material. It is argued that combining a nanoscale aperture with a high-speed MEMS shutter enables single atom placement. The ability to deposit in situ and without the need for resists and etchants, allows for bottom-up patterning using many materials that are chemically incompatible with electron beam lithography. Typical examples would be alkali metals such as lithium as well as other reactive elements like sulfur.

Other resist-free, direct nanopatterning techniques exist. Dip pen nanolithography is a technique based on using an atomic force microscopy (AFM) probe to flow liquid “inks” onto a substrate,[3] and oxidation nanolithography that alters the local chemistry[4−6] as summarized by Tseng.[7] Both methods are impressive, though limited by the types of compatible deposition materials and operation environments. Stencils can be used for resist-free deposition.[8,9] In such methods, the patterned geometry is an exact copy of the stencil. This approach cannot be used for depositing topologically complex structures, as the plate must be simply connected. As a consequence, topological structures with holes, such as a ring or loop, cannot be patterned. Most similar to our approach, apertures or stencils can also be placed on an AFM cantilever or another micropositioner and used for resist-free patterning of arbitrary shapes.[10−12] These systems lack the integrated shutter and speed made possible with MEMS devices and do not allow for large arrays of devices to be written in parallel. Their setup and control is also significantly more complex, making it difficult to integrate these techniques with other technologies.

MEMS devices have been successfully demonstrated in a wide range of operating conditions. They are robust, can operate at cryogenic temperatures, and are highly reliable.[13] In situ deposition can be used for ultraclean quench-condensed films made of reactive elements and compounds.[14] Using a relatively simple control circuit, electrostatic actuation allows for high displacement resolution and negligible power consumption. The MEMS writers themselves are manufactured in a foundry at low cost using industry standard lithography methods in a scalable way. Because of their low cost and batch fabrication, our approach allows for the scalable manufacturing of large numbers of nanodevices. The chips are single use devices enabling high flexibility and turnover. They are simple to operate and inexpensive so nonexperts can rapidly fabricate

Received: May 9, 2013
Revised: June 18, 2013

 © XXXX American Chemical Society dx.doi.org/10.1021/nl401699w | Nano Lett. XXXX, XXX, XXX−XXX

their nanoscale devices to study novel materials or NEMS structures.

MEMS technology is expanding at a tremendous rate. Current systems include gyroscopes, mass sensors, accelerometers, pressure sensors, switches, time standards, and more.[15−17] Because of the large linear response regime of polysilicon, there is practically no mechanical fatigue, enabling a high cycling number and rate with no hysteretic effects. The small size scale results in a high mechanical frequency while retaining a high quality factor. Therefore, to a large extent, the writers are intrinsically mechanically isolated from their surroundings and external vibrations, making them easier to use in a wide range of applications without the need for elaborate vibration isolation.

Device Design and Fabrication. Our devices are fabricated using the MEMSCAP PolyMUMPs[18] process, described in the Supporting Information (Figure S1). Such optical lithography based structures can be manufactured economically at a large scale with ∼1 μm resolution. The individual writers, consisting of electrostatic comb actuators, folded springs and a central plate, sit on a 2.5 × 2.5 mm^2 die stack of 600 nm silicon nitride and doped silicon handle 675 μm thick. Figure 1 depicts micrographs of the structure and its components. The central plate is suspended over the substrate by four doubly folded flexure springs and tethers. The springs and tethers can be combined into a single device that can move laterally >10 μm in all four quadrants, using the substrate as an additional electrode enables z-axis pull in. This design is similar to MEMS based nanopositioners described in the literature using both comb[19−21] or piezoelectric actuation methods.[22] The smallest feature or dot that can be patterned is defined by the aperture dimension. We use a FIB to mill an aperture in the plate of the writer. By leveraging the strengths of the scalable PolyMUMPs process with the nanoscale resolution of a FIB we obtain MEMS devices 2 mm across with customized feature sizes below 50 nm.

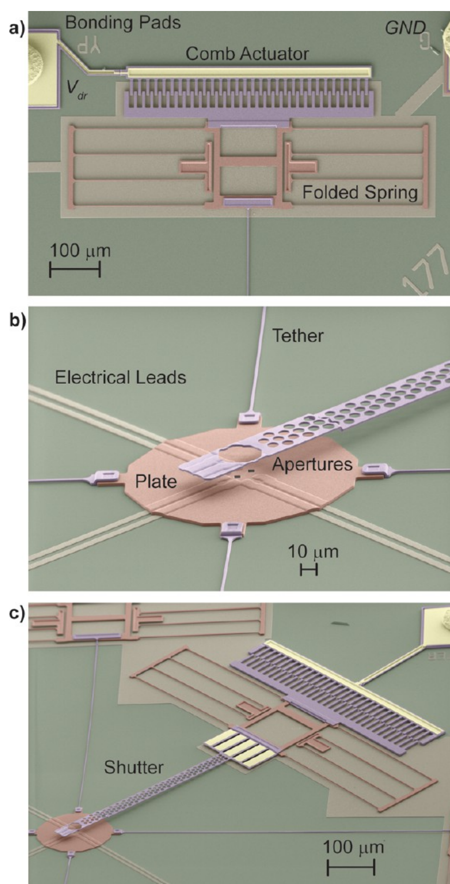

Figure 1. False color SEM micrographs of the MEMS writer. (a) Electrostatic comb actuator (F = 0.924(nN)/(V^2) × V^2) and folded springs (k = 0.335 N/m). Preset leads enable electrical access. (b) Plate with apertures. Aperture diameter ranges from 0.05−2 μm. Tethers connect the plate to the folded springs. (c) Double plate design. Top plate functions as a high-speed shutter.

The aperture milling is accomplished by a two-step process illustrated in Figure 2. The thinner the plate, the smaller the aperture can be made (as a high-aspect ratio reduces the milling resolution, without an etch-enhancing gas a typical trench aspect ratio is approximately four[23]). For this reason initially a 4 × 4 μm^2 large trough is milled 1.0−1.3 μm through the 1.5 μm plate. This also smooths the polysilicon. As a result, it becomes possible to poke an aperture smaller than 50 nm through the remaining 200−300 nm of silicon. In principle, this process could be optimized to produce apertures in diameter just above the gallium ion beam size, which can be as small as ∼5−10 nm.[24,25] Even smaller pinholes (possibly down to less than 10 nm) can be manufactured using a transmission electron microscope (TEM), provided the silicon is sufficiently thinned.[26] Figure 2e depicts the atom flux path from the source to the canvas though the milled aperture.

Experimental Methods. The MEMS device is packaged and ball bonded into an 8 pin DIP chip holder and covered with a lid containing a ∼75 μm hole centered over the plate. The device is actuated by four electrostatic comb drives, each attached to a folded spring. See Supporting Information Figures S2−S5 for a full discussion of the electromechanical response of the device. Patterning is conducted in a thermal evaporator at pressures in the mid 10^{-6} Torr range (Supporting Information Figure S6). Feedthroughs enable electrical access to the writer. Gold is deposited through the apertures as the MEMS writer is actuated by four independent voltage sources; an additional fifth source actuates the shutter, and a sixth can be used for adjusting the plate height.

For a typical deposition, a crucible is heated resistively until a stable gold flux of 0.20−0.25 nm/s is obtained, corresponding to ∼2 monolayers per second. The desired pattern is converted into the corresponding voltage coordinates; where for each axis a separate voltage source is used. Whenever actuating in one direction, the voltage on the opposite capacitor is set to zero. Depending on the desired pattern, a single pass or multiple passes are performed during a 10−20 min period. Where the total deposition may be 300 nm due to the motion of the aperture over the traced area, the pattern itself is typically less than 10 nm thick. The deposition rate was chosen to allow for fast multipass deposition traces or a single slow pass. In principle the deposition rate could be considerably increased or decreased, obtaining the same results for corresponding corrections to the aperture speed. The thickness of the deposited metal on the nitride is the product of the evaporation rate and the effective time the aperture is over a given point. This time can be adjusted by changing the speed of the central plate or the number of passes. A macroscopic shutter protects the MEMS during the ramping of the source temperature. Some versions of our devices include a MEMS shutter only micrometers over the apertures enabling high speed opening and closing of individual apertures on a single plate. Essentially,

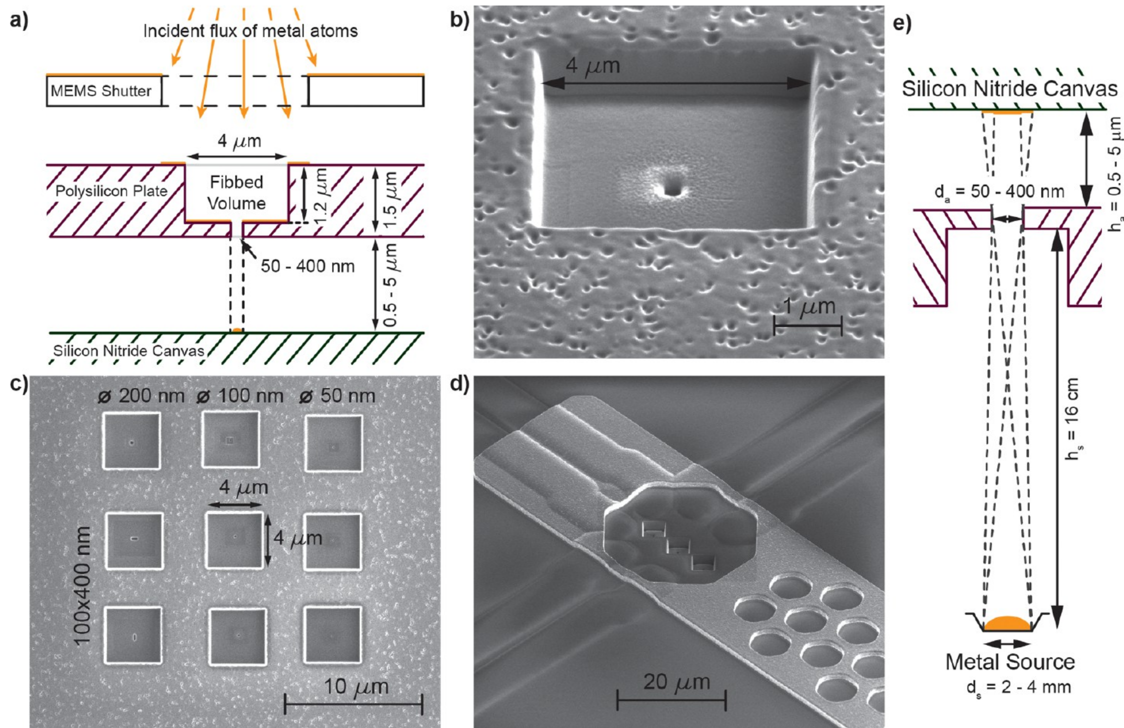

Figure 2. Aperture fabrication. (a) Diagram of milled aperture, including source, shutter, and silicon nitride canvas. (b) Two step aperture. Initial $4 \times 4 \times 1.2\ \mu m^3$ trough thins and smooths the polysilicon plate. High-precision mill pokes through to make the 200 nm scale aperture. (c) Array of apertures with various sizes and shapes, close-up of top left aperture is depicted in panel b. (d) Prerelease plate, shutter, and apertures. (e) Source−aperture−canvas geometry illustrates the path of the atomic flux.

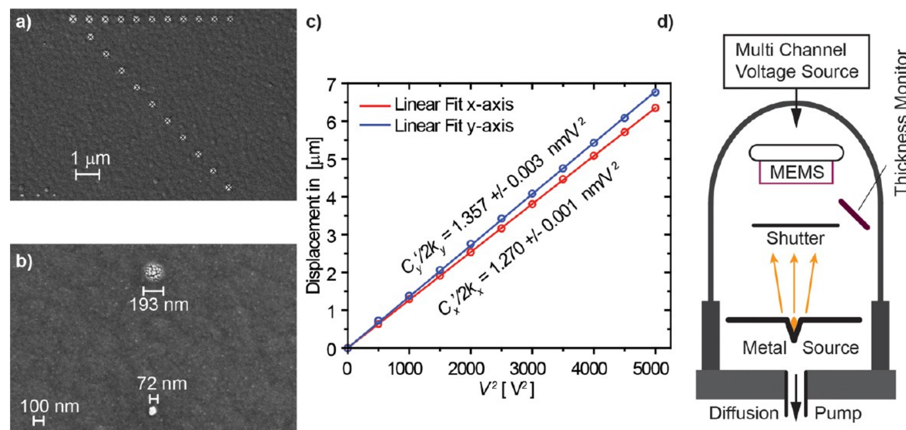

Figure 3. $x-y$ and z-axis control. (a) SEM micrograph of 200 nm dots placed along x and $x-y$ axis for equal spacing in V^2. (b) SEM micrograph of two dots deposited through a 100 nm aperture. Top was deposited with large canvas−aperture spacing ($h_a \approx 5\ \mu m$), bottom dot deposited after pull in ($h_a \approx 0.5\ \mu m$). (c) Displacement versus V^2 plot for x- and y-axis. The linear fit illustrates the electromechancial response $(C_x')/(2k_x) = 1.270 \pm 0.001$ nm/V^2 and $(C_y')/(2k_y) = 1.357 \pm 0.003$ nm/V^2 along the x- and y-axis respectively. (d) Experimental setup. Includes thermal evaporator, multichannel voltage source, thermal evaporator, and MEMS writer.

any compound that can be evaporated in vacuum could serve as a source material, especially if only a small number of atoms are desired. Here, for simplicity, a resistive thermal evaporator was used. This method would work with other deposition methods including electron-beam evaporation multiplying the number of types of sources that can be used.

Electromechanical Response of the Plate. Figures 3 through 6 demonstrate the technological capabilities of the MEMS device. Figure 3 depicts the electromechancial response in the $x-y$ axis as well as the blurring effect through z control. The experimental setup is outlined in Figure 3d. The electrostatic force

$$F_i = -\frac{dE}{dx_i} = -\frac{V^2}{2}\frac{dC}{dx_i} \tag{1}$$

is balanced by the restoring force of the folded flexural springs and tethers

$$F_i = k_i x_i = 2(k_{\text{foldedspring}\,i} + k_{\text{tether}\,i})x_i \tag{2}$$

where the tethers contributing to the spring constant along the x-axis are attached to the folded flexure springs that determine the spring constant along the y-axis (and vice versa). A complete discussion is given in the Supporting Information.

dx.doi.org/10.1021/nl401699w | *Nano Lett.* XXXX, XXX, XXX−XXX

Combining the electrostatic and mechanical properties results in the displacement-voltage relation

$$x_i = -\frac{C'}{2k}V^2 \tag{3}$$

where $C_i' = (dC)/(dx_i)$ is the derivative of the capacitance of the comb drive along the direction of actuation. This relationship is reproduced in Figure 3c with very high precision. Over the entire displacement range measured there are no observed deviations from the linear elastic response. The V^2 displacement dependency results in a low-voltage regime where displacements around the origin can be set with high precision and electrical noise does not couple into the mechanical response. At the same time, larger displacements of up to 10 μm are still possible with voltages below 100 V. The variations in the electromechanical response of the *x*- and *y*-axes are explained by small changes of the geometry of the tethers and springs. As $k_i \sim (tw^3)/(L^3)$ only a 3% change in the width of the springs (corresponding to 60 nm) is sufficient to explain the observed variations of the electromechancial response of the *x* and *y*-axes.

In Figure 3b, two dots deposited with the same aperture are depicted. The variation in diameter and edge sharpness is a result of changes in the aperture−canvas distance. The atom flux path for this setup is illustrated in Figure 2e. The doped substrate beneath the nitride forms a capacitor with the central plate. Applying a voltage will pull the plate toward the substrate. This allows the distance to be tuned from 5 to 3.7 μm or pulled all the way in for contact lithography, resulting in a sharper dot. Stiction between the plate and substrate prevent the plate from returning to its original position after pull-in. Hence, this method to obtain sharper edges is only suited for the last position of the aperture. At the (0,0) position the plate is ∼5 μm above the substrate. After an initial deposition the plate is moved by 1 μm and pulled down to the substrate. The resulting dots are ∼193 and 72 nm in diameter. The 121 nm narrowing is explained by the reduction in geometric smearing, eliminating vibration (from an estimated amplitude of 12 nm to zero as the plate is no longer free to move relative to the substrate) and aperture filling as described below.

Atomic Calligraphy. Figure 4 depicts rings traced out by different sized apertures. The smallest structure shown is a ring with a radius of 100 nm and a line width of just under 90 nm, drawn with a 50 nm aperture. Figure 4a, exhibits a ring drawn off center with the zero voltage location marked by a dot resulting from the stationary aperture. These images illustrate the high level of control and reproducibility. Even after 10 passes, the rings are traced out identically over the first pass. In addition to mechanical vibration, the fuzziness of the edge is the result of geometric effects due to the height of the aperture over the substrate (Supporting Information Figure S7). This sets a limit to the resolution of the device and can be improved by pulling the plate toward the nitride. Figure 5 depicts an array of nine 4.76 × 2.84 μm^2 infinity symbols patterned in parallel with differently shaped apertures. All apertures are on the same plate so the deposition occurs in parallel. A larger array printed from 4 × 4 identically milled apertures is shown in Supporting Information Figure S9. Figure 5b illustrates how rotating the rectangular aperture results in different line widths and thicknesses depending on the direction in which the plate moves. The resulting trace looks like a Moebius loop written by atomic calligraphy, analogous to the nib of a fountain pen. Such

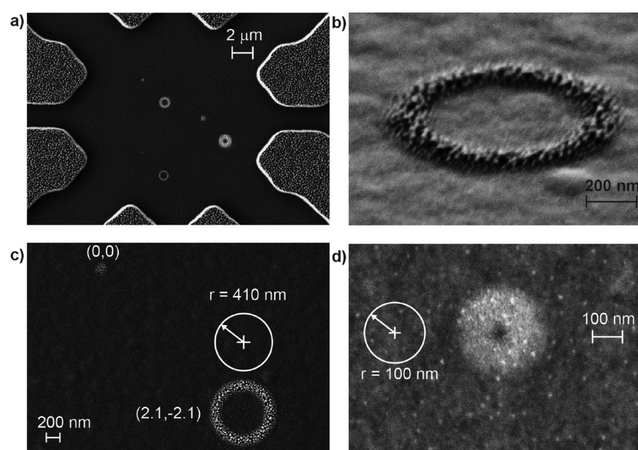

Figure 4. Demonstration of deposited rings of gold. (a) A plate with three apertures of varying sizes (100, 200, and 400 nm) illustrates rings deposited off center, where the dots indicated the zero voltage position. (b) Close-up of 400 nm radius ring of the 100 nm aperture structure, positioned at (2.1,−2.1) μm. (c) Top down view of the same structure as in (b) including the (0,0) position. (d) Shown is a 100 nm radius ring traced using a 50 nm aperture, resulting in a line width of 88 nm.

apertures can be used selectively to pattern narrow or broad structures by choosing the direction of motion.

The FIB dictates the smallest aperture that can be manufactured. The smallest aperture used to date resulted in an evaporated gold "pixel" size of ∼42 × 57 nm^2, and using chromium a pixel size of ∼50 × 34 nm^2 was achieved, as depicted in Supporting Information Figure S8. It is possible to narrow the aperture by selectively allowing it to fill in with the deposition metal, as illustrated in Figure 5c. During the deposition, the aperture was moved in a straight line. As the hole fills in the trace becomes narrower. This process is analogous to the "ion-beam sculpting" used for the fabrication of molecular sized nanopores.[27] The narrowest line eventually blurs out and is no longer discernible. The lower limit of the line width is dictated by height of the aperture above the nitride as well as the level of mechanical vibration. For this case, using gold as a deposition material the aperture diameter shrinks by ∼0.87 times the total deposition thickness. An AFM image of a similar, though slightly large structure, is included in Figure S12 of the Supporting Information. It is clearly visible how the line narrowing also leads to thinner structures. This is a direct result of the thickness-aperture size relation for a moving plate discussed previously. The pore fills in much faster than would be expected by purely geometric considerations, as has been reported for stencil masks.[9] It is suggested that surface phenomena result in the movement of the gold "adatoms" that are subsequently trapped in the hole, which is thereby closed. It is expected that the deposition material, deposition rate, source-MEMS geometry and plate temperature all contribute to the rate of closing. Where the closing of the aperture sets an upper limit on the total amount of material that can be pattered, it also allows for the controlled narrowing of the aperture. To reach the atomic scale, a feedback mechanism must be implemented.[27] In a device printing process, the narrowing would be the penultimate step, hence in situ customizing the aperture before the smallest feature is patterned. In operation, we envision using an array of holes, writing larger structures first with larger apertures. The smaller

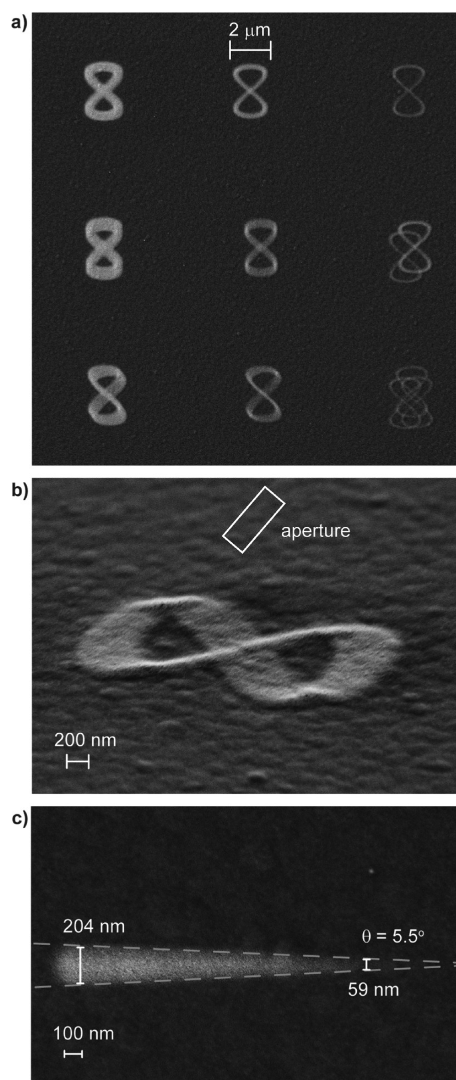

Figure 5. Results: Arrays, Moebius loops and line sharpening. (a) Array of apertures of varying sizes and shapes. The center and bottom right structures are made with two and three adjacent apertures respectively. (b) Tilted image of gold deposited through a tilted aperture results in an image of a Moebius Loop. Using this calligraphy method, the width of the line depends both on the shape of the aperture and its orientation relative to the direction of the motion of the plate. (c) Aperture thinning. As gold is deposited the aperture fills in. This process can be used to controllably narrow apertures of varying sizes. Depositing 260 nm of gold results in a narrowing of the trace by ∼225 nm. An initially 204 nm diameter line is closed completely with deposition still visible below 60 nm. The rate of closing and minimum feature discernible is defined by the material used as well as the source-aperture-canvas geometry (Figure 2e).

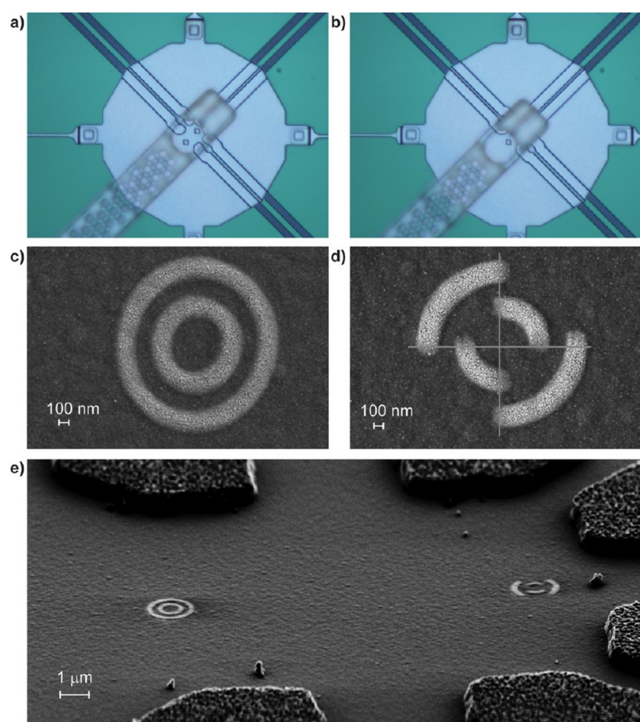

Figure 6. Plate and shutter device. Optical image of (a) open shutter (V_{SH} = 40 V) with two apertures visible and (b) closed shutter (V_{SH} = 70 V) with one aperture visible. (c) Concentric circles drawn by a continuously open aperture. (d) Truncated concentric circles resulting from the opening and closing aperture. (e) Concentric circles side by side illustrate MEMS shutter functionality.

holes are kept clean with the shutter until needed. Alternatively, longer stencil life has been reported by adding a local heater to the aperture, removing unwanted deposition from the source metal on the stencil.[12]

We have integrated an on chip MEMS shutter within a few micrometers over the plate in order to control when an aperture is open or shut with high temporal and spatial precision. The open and closed positions of the shutter are depicted in Figure 6a,b, respectively. This corresponds to comb potentials of 40 and 70 V. To demonstrate the ability to open and close a single aperture in a two aperture plate, a set of concentric circles are drawn with 400 and 800 nm radii. The shutter is set to open and close so that each circle is truncated into four quadrants. The resulting pattern for the aperture that is always open is depicted in Figure 6c. The corresponding deposition through the second aperture, which is selectively closed, is illustrated in Figure 6d. Figure 6e is a SEM (scanning electron microscope) micrograph of the adjacent patterns. These depositions resulted from 11 passes, illustrating the repeated opening and closing of the shutter a total of 44 times. Though here the speed of the shutter is not demonstrated, in principle the rate is determined by the resonant response, resulting in an open-closed cycle of ∼100 μs period. Methods to reduce this time scale are discussed in the Supporting Information (Figure S10).

Discussion. The resolution of the MEMS writer is determined by the electronic control circuit, as well as the electrical and mechanical noise. As the displacement resulting from the applied voltage is given by eq 3 the displacement sensitivity with respect to the voltage is $dx = (1/k)(dC/dx)V\,dV = 2.54 \times 10^{-3}\ (\mu m)/(V^2)V\,dV$. This means that at 1 V actuation and a voltage noise as high as 1 V would result in only 2.54 nm displacement noise. At 100 V actuation, corresponding to a displacement of x = 12.7 μm, and a voltage noise of 10 mV the resulting displacement noise is still only 2.54 nm, well below our detection resolution at this time. The high quality factor and resonance frequency isolates the mechanical mode from external vibration noise which typically falls off as $1/f$. Current estimates based on measurements indicate typical vibrations are on the order of 10−40 nm. Pulling the central plate down to the substrate sharpens the deposited structures. The primary effect of the pull down is to eliminate any geometric smearing due to the finite source size (Figure 3).

Furthermore, any mechanical motion due to electrical or vibrational noise is eliminated once the plate makes contact with the substrate and can no longer move independently. Surface diffusion that clogs the aperture may also broaden the features.[9] Adding full control of the plate height will enable control of the geometric smearing depending on the application. Dynamic smearing will occur due to the ring down time of the structure (Supporting Information Figure S11). This can be compensated using slow small step sizes and active feedback control.[28]

Considering the small apertures, low evaporation rates, and high shutter speeds, we predict it is possible to allow stochastically a single atom to pass through the aperture. Evaporating with a deposition rate of one monolayer per second means approximately 34 300 gold atoms are passing through a 50×50 nm^2 aperture every second. Since the shutter can open and close in under 100 μs, it is estimated that just over 3 atoms can pass per cycle. Using smaller apertures, lowering the deposition rate and driving the shutter above its resonance speed are all possible and will push the average number of atoms passing though the aperture to of order one.

Conclusions. In summary, we present a novel MEMS-based mask writer. By customizing optical lithography-based MEMS devices with a focused ion beam, we mill apertures in a plate that can be controlled dynamically over a 20×20 μm^2 area. Using this device we pattern structures with feature sizes <50 nm. As the patterning method described here is the final fabrication step, this technology can be used to build electronic circuits and structures in situ out of materials typically not used in nanolithography. An integrated MEMS shutter makes it possible to control stochastically the number of atoms passing through the aperture down to of order one. The small footprint of this MEMS device, as well as the thermal and mechanical properties of polysilicon, allow this technology to be implemented directly in a cryogenic environment. Integrating this writer together with a MEMS based evaporator, as well as resonant sensors for deposition rate and temperature creates a cheap and versatile "fab on a chip". This will enable new mesoscopic experiments of quench condensed films, quantum dots, and single atom effects.

■ ASSOCIATED CONTENT

Supporting Information

This document contains technical information on the MEMS device, the experimental setup, and analysis of the results. In addition, two short video materials are included to illustrate the motion of the plate and shutter system. This material is available free of charge via the Internet at http://pubs.acs.org.

■ AUTHOR INFORMATION

Corresponding Author

*E-mail: djb1@bu.edu. Tel: +1 617 358-4080. Fax: +1 617 353-7337. Address: 8 Saint Mary's Street, Boston, MA 02215, U.S.A.

Author Contributions

The manuscript was written through contributions of all authors. All authors have given approval to the final version of the manuscript.

Notes

The authors declare no competing financial interest.

■ ACKNOWLEDGMENTS

The authors thank Vladimir Aksyuk for help with the MEMS designs and discussions on the electromechanical response of these systems and Gregory McMahon for technical assistance with the FIB used to fabricate the apertures. This research is funded in part by Boston University.

■ ABBREVIATIONS

FIB, Focused ion Beam; MEMS, microelectromechanical system; NEMS, nanoelectromechanical system

■ REFERENCES

(1) Ito, T.; Okazaki, S. *Nature* **2000**, *6799*, 1027−1031.

(2) Grigorescu, A.; Hagen, C. *Nanotechnology* **2009**, *29*, 292001.

(3) Piner, R. D.; Zhu, J.; Xu, F.; Hong, S.; Mirkin, C. A. *Science* **1999**, *5402*, 661−663.

(4) Meister, A.; Liley, M.; Brugger, J.; Pugin, R.; Heinzelmann, H. *Appl. Phys. Lett.* **2004**, *25*, 6260−6262.

(5) Garcia, R.; Martinez, R. V.; Martinez, J. *Chem. Soc. Rev.* **2005**, *1*, 29−38.

(6) Dagata, J.; Schneir, J.; Harary, H.; Evans, C.; Postek, M.; Bennett, J. *Appl. Phys. Lett.* **1990**, *20*, 2001−2003.

(7) Tseng, A. A. *Nano Today* **2011**, *5*, 493−509.

(8) Van Den Boogaart, M.; Kim, G.; Pellens, R.; Van Den Heuvel, J.; Brugger, J. *J. Vacuum Sci. Technol., B* **2004**, *6*, 3174−3177.

(9) Deshmukh, M. M.; Ralph, D.; Thomas, M.; Silcox, J. *Appl. Phys. Lett.* **1999**, *11*, 1631−1633.

(10) Luthi, R.; Schlittler, R. R.; Brugger, J.; Vettiger, P.; Welland, M. E.; Gimzewski, J. K. *Appl. Phys. Lett.* **1999**, *9*, 1314−1316.

(11) Champagne, A.; Couture, A.; Kuemmeth, F.; Ralph, D. *Appl. Phys. Lett.* **2003**, *7*, 1111−1113.

(12) Savu, V.; Xie, S.; Brugger, J. *Nanoscale* **2011**, *7*, 2739−2742.

(13) Bolle, C.; Aksyuk, V.; Pardo, F.; Gammel, P.; Zeldov, E.; Bucher, E.; Boie, R.; Bishop, D.; Nelson, D. *Nature* **1999**, *6731*, 43−46.

(14) Bishop, D.; Dolan, G. *Phys. Rev. Lett.* **1985**, *26*, 2911−2914.

(15) Judy, J. W. *Smart Mater. Struct.* **2001**, *6*, 1115.

(16) Lopez, D.; Pardo, F.; Bolle, C.; Decca, R.; Bishop, D. *J. Low Temp. Phys.* **2004**, *1*, 51−62.

(17) Bishop, D.; Pardo, F.; Bolle, C.; Giles, R.; Aksyuk, V. *J. Low Temp. Phys.* **2012**, 1−14.

(18) MEMSCAP. http://www.memscap.com/products/mumps/polymumps/reference-material, 2012 (accessed 2/20/2012).

(19) Ji, L.; Zhu, Y.; Moheimani, S. O. R.; Yuce, M. R. A micromachined 2DOF nanopositioner with integrated capacitive displacement sensor. *IEEE Sens.* **2010**, 1464−1467.

(20) Liu, X.; Kim, K.; Sun, Y. *J. Micromech. Microeng.* **2007**, *9*, 1796.

(21) Pang, C. K.; Lu, Y.; Li, C.; Chen, J.; Zhu, H.; Yang, J.; Mou, J.; Guo, G.; Chen, B. M.; Lee, T. H. *Mechatronics* **2009**, *7*, 1158−1168.

(22) Polit, S.; Dong, J. *IEEE/ASME Trans. Mechatronics* **2011**, *4*, 724−733.

(23) Yao, N. *Focused ion beam systems: basics and applications*; Cambridge University Press Cambridge: New York, 2007.

(24) Langford, R. M.; Nellen, P. M.; Gierak, J.; Fu, Y. *MRS Bull* **2007**, *5*, 417−423.

(25) Watt, F.; Bettiol, A.; Van Kan, J.; Teo, E.; Breese, M. *Int. J. Nanosci.* **2005**, *03*, 269−286.

(26) Storm, A.; Chen, J.; Ling, X.; Zandbergen, H.; Dekker, C. *Nat. Mater.* **2003**, *8*, 537−540.

(27) Aziz, M.; Golovchenko, J.; Branton, D.; McMullan, C.; Stein, D.; Li, J. *Nature* **2001**, *6843*, 166−169.

(28) Borovic, B.; Liu, A.; Popa, D.; Cai, H.; Lewis, F. *J. Micromech. Microeng.* **2005**, *10*, 1917.